catalysts

MDPI

Article

Effects of CO and H_2O Co-Feed on the Adsorption and Oxidation Properties of a Pd/BEA Hydrocarbon Trap

Ryan Zelinsky and William S. Epling *

Department of Chemical Engineering, University of Virginia, Charlottesville, VA 22904, USA; rpz3ub@virginia.edu
* Correspondence: wsepling@virginia.edu; Tel.: +1-434-924-6278

Abstract: Hydrocarbon traps for exhaust emissions control adsorb hydrocarbons in low temperature exhaust and release them as the exhaust warms up. In this work, a Pd/BEA hydrocarbon trap was tested under lean exhaust conditions using ethylene and dodecane as model hydrocarbons. Ethylene uptake was partially inhibited by CO and H_2O when fed separately. When both were added, the loss in ethylene uptake was 90% relative to the condition with no H_2O or CO. Dodecane uptake was unchanged under all conditions tested. During a temperature ramp, ethylene desorbed and was combusted to CO_2 and H_2O over active Pd centers. Further, oxidation light-off of dodecane generated an exotherm which caused rapid desorption of the remaining hydrocarbon species from the zeolite. For both hydrocarbons, CO co-feed led to a decreased oxidation light-off temperature, and therefore lower desorption temperature. By pretreating the catalyst in CO and H_2O at 80 °C, and even after removing CO from the feed, the enhanced oxidation light-off behavior was observed. DRIFTS characterization shows that some form of oxidized Pd was reducible to Pd^0 by CO at 80 °C only in the presence of H_2O. Further, this reduction appears reversible by high temperature oxygen treatment. We speculate that this reduced Pd phase serves as the active site for low temperature hydrocarbon oxidation.

Keywords: palladium zeolite; hydrocarbon trap; emissions control; cold start emissions

Citation: Zelinsky, R.; Epling, W.S. Effects of CO and H_2O Co-Feed on the Adsorption and Oxidation Properties of a Pd/BEA Hydrocarbon Trap. *Catalysts* **2021**, *11*, 348. https://doi.org/10.3390/catal11030348

Academic Editors: Maria Casapu and Dmitry E. Doronkin

Received: 24 January 2021
Accepted: 3 March 2021
Published: 8 March 2021

1. Introduction

Emerging combustion technologies present new challenges for emissions control. Low temperature combustion (LTC) diesel engines, of interest due to their increased fuel economy, create a different pollutant profile which is higher in hydrocarbon and CO emissions, but lower in NO_x and soot, than their traditional standard combustion mode counterparts [1]. The combination of lower exhaust temperatures and increased CO and hydrocarbon emissions will test current diesel oxidation catalyst (DOC) technologies, which require temperatures above 250 °C for adequate conversion of unburned hydrocarbons [2]. Additionally, it is estimated that between 60–80% of total hydrocarbon emissions occur during the cold-start period [2,3]. With the onset of Tier 3 standards from the Environmental Protection Agency (EPA), which reduce the allowed amount of non-methane organic (NMOG) + NO_x emissions from light and medium duty vehicles to below 0.30 mg/mi by 2025, additional consideration for cold-start hydrocarbon emissions is required. These trends and regulations point to the need for new aftertreatment technologies.

A proposed solution to reduce hydrocarbon emissions is the hydrocarbon trap. A hydrocarbon trap selectively adsorbs hydrocarbons during low temperature periods. As the exhaust warms up, the hydrocarbons are then released from the trap. An effective hydrocarbon trap would release the stored molecules after reaching a temperature appropriate for oxidation by the DOC (>250 °C) or by an integrated oxidation catalyst within the trap itself. Although the hydrocarbons should be released after the DOC is active, they should not be retained to too high of a temperature so that the hydrocarbon trap can be regenerated before the next cold-start cycle.

Zeolites have received the majority of the attention for this application due to their properties as molecular sieves, hydrothermal stability, and solid acid behavior [4–11]. For diesel exhaust applications, zeolite beta (BEA) is often studied. This is due to its large diameter pores (5.95 Å) [12] which allow for physisorption of larger molecules typical of diesel exhaust such as dodecane (4.3 Å) and toluene (5.85 Å) [13]. More recently, metal ion-exchanged zeolite hydrocarbon traps have been studied due to their increased effectiveness in adsorbing unsaturated hydrocarbons such as ethylene, propylene, and toluene via chemisorption onto the metals [10,14–19]. Due to competition by water, alkenes are generally not appreciably adsorbed over the H^+ form of most zeolites under wet conditions [8]. Kang et al. found that the addition of Ag to the framework could enhance the trapping capacity of BEA towards ethylene, however these improvements were completely lost in the presence of water [15]. The addition of Pd to the framework however gives some resistance to water inhibition of ethylene adsorption, as reported by Xu et al. [20].

Palladium-doped zeolites seem to provide unique advantages over other metals. First, Pd ions are adsorption centers for unsaturated hydrocarbons which expands the trapping capabilities of the zeolite [21]. Additionally, Pd serves as an oxidation catalyst which can oxidize the incoming and trapped hydrocarbons and can impact the desorption properties due to the exotherm generated when hydrocarbons are oxidized [16]. Additionally, in the high oxygen environment of diesel exhaust, the catalytic oxidation supports regeneration of the hydrocarbon trap, oxidizing residual hydrocarbon species. This can be important, as for example ethylene and propylene are known to undergo oligomerization reactions involving zeolite Brønsted acid sites which can lead to catalyst deactivation [20,22].

The hydrocarbon trap must be active when exposed to the wide variety of species that comprise diesel exhaust. This includes ppm levels of pollutants such as CO, short and long chain olefins and paraffins, aromatics, SO_x, NO_x, and others. Additionally, H_2O and CO_2 are present in percent levels. Prior work shows that NO and H_2O adsorb competitively with olefins and aromatics to both Brønsted acid sites and ion-exchanged Cu, Fe, and Pd sites [5,7,23]. Literature also suggests that competition between different hydrocarbon classes may not always be significant, for example dodecane does not compete with ethylene adsorption, due to different uptake mechanisms [16].

CO is also known to adsorb to the Pd species which exist in a zeolite. Prior diffuse reflectance Fourier transform infrared spectroscopy (DRIFTS) studies on Pd/BEA exposed to CO indicate that at 80 °C, CO is bound as CO–Pd^0, CO–Pd^+, and CO on two Pd^{2+} forms, Z^-–Pd^{2+}–Z^- and Z^-–$Pd(OH)^+$ where Z^- is a cation exchange site [24,25]. CO–Pd^+ and CO–Pd^0 species may stem from reduction of Pd^{2+} by the probe molecule [25–27]. In studies with Pd/BEA and Pd/SSZ-13, bridging CO-$Pd_2{}^0$ was also observed indicating the presence of particles [24,28]. In the context of a zeolite passive NO_x adsorber (PNA), when CO was co-fed with NO to Pd/BEA, it has been proposed that a stable mixed palladium(II) carbonyl-nitrosyl complex, (NO)(CO)–Pd^{2+}, formed, which was found to change NOx storage characteristics [29]. In addition to adsorbing to and altering the chemical state of Pd, several studies have shown that CO exposure induces degradation of exchanged Pd in zeolite PNAs [26,30,31] which has been attributed to Pd reduction [26,31] and Pd particle formation [26]. Such an effect was not seen with other reductants, such as C_2H_4 or H_2 [31].

In this work, the adsorption-desorption properties of a 1% by weight Pd/BEA hydrocarbon trap were examined under a simulated diesel exhaust gas mixture. The role of CO was investigated using in situ DRIFTS and adsorption-temperature programmed oxidation (TPO) studies, while the catalyst was further characterized by H_2 temperature programmed reduction (TPR). The results indicate that during adsorption, CO inhibits hydrocarbon uptake over ionic Pd active sites. CO in the presence of H_2O also led to the formation of reduced Pd species which enhanced hydrocarbon oxidation during the TPO phase.

2. Results and Discussion

2.1. H_2 TPR

Hydrogen TPR is commonly used to characterize the initial state of the Pd species in Pd-exchanged zeolites and was used here to describe the distribution of Pd particles vs. ions. Figure 1 shows the H_2 TPR plot for the 1% Pd/BEA sample used in this study.

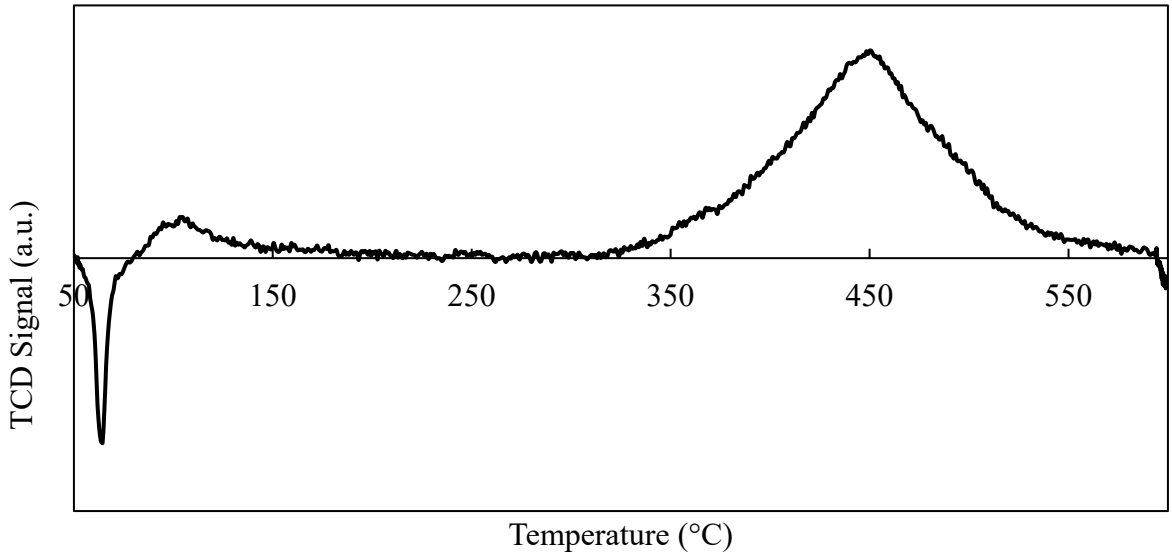

Figure 1. Hydrogen TPR for 1% Pd/BEA (5% H_2/He, Ramp rate = 10 °C/min) Pretreatment: 500 °C in 10% O_2/He for 60 min.

The negative peak at 50–80 °C represents H_2 production and originates from the decomposition of PdH, which is formed during the initial H_2 exposure at 50 °C before the temperature ramp. The PdH phase forms when H_2 reacts with particulate Pd and is thus an indicator of its presence [32]. The peak at 80–150 °C and the high temperature peak at 450 °C correspond to different forms of ionic Pd [26,30]. The H_2 TPR results demonstrate that this catalyst is not completely ion-exchanged and contains both ionic and particulate Pd. This sample is representative of the expected Pd/BEA state after several engine cycles. This is because recent literature has indicated that a catalyst which has been exposed to CO at high temperatures will experience partial Pd agglomeration to an irreversible extent, resulting in a mix between cationic Pd and agglomerated particulate Pd [26,30,31].

2.2. Ethylene and Dodecane Adsorption

Ethylene and dodecane were used as surrogate hydrocarbons to test the adsorption capacity and desorption characteristics of the Pd/BEA hydrocarbon trap. Ethylene was chosen to represent short chain olefins, which are a considerable portion of hydrocarbon emissions, even from a diesel engine [33].

Figure 2 displays the transient uptake of ethylene over Pd/BEA under four experimental conditions. The hydrocarbon-containing gas stream was switched from the bypass to the reactor at t = 50 s. The summarized uptake capacities are listed in Table 1. The trend with respect to H_2O is in good agreement with Xu et al. [20], as we observe some ethylene uptake in the presence of H_2O, however less than that observed in the dry case. Ethylene uptake occurs over both Brønsted acid sites and cationic Pd. In the absence of H_2O, Brønsted acid sites are free to interact with π-electrons in unsaturated hydrocarbons, however when H_2O is present in such a high concentration it outcompetes ethylene for these sites [8,34].

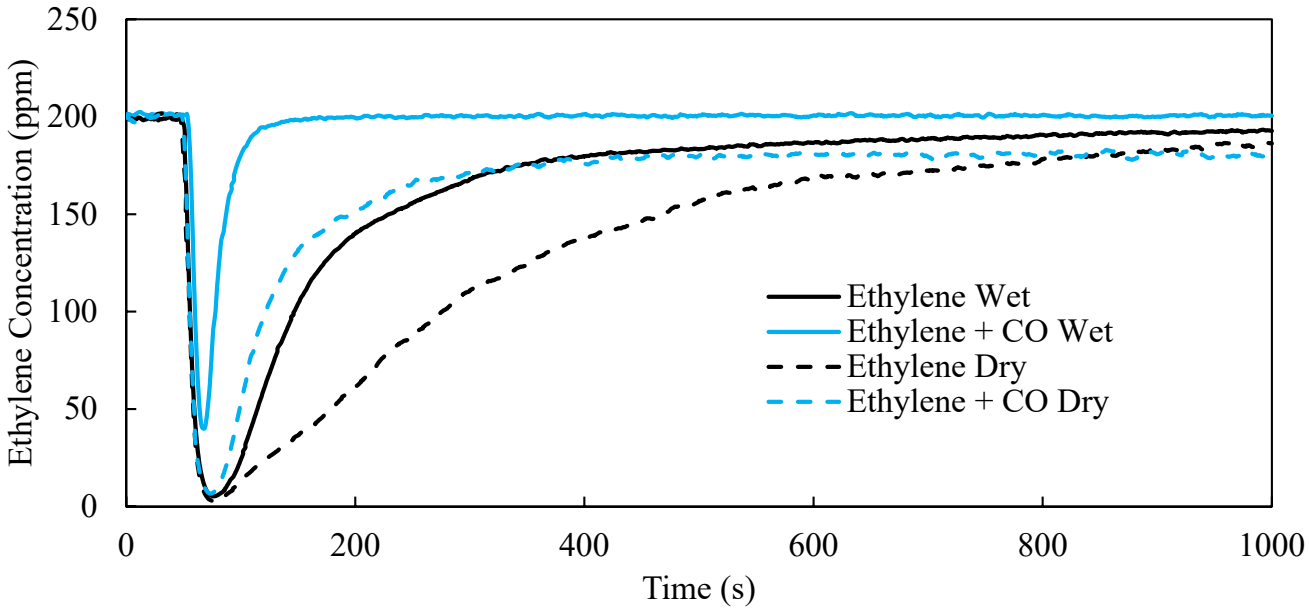

Figure 2. Ethylene uptake over 1% Pd/BEA with and without CO co-feed in wet and dry conditions. Adsorption begins at T = 50 s. (200 ppm ethylene, 0 or 500 ppm CO, 0 or 6% H_2O, 12% O_2, balance N_2).

Table 1. Ethylene uptake and ethylene/Pd ratio for each experiment.

Experiment	Ethylene Uptake (μmol)	Ethylene/Pd Ratio
Ethylene Dry	47	3.6
Ethylene + H_2O	24	1.8
Ethylene + CO Dry	31	2.4
Ethylene + H_2O + CO	3.5	0.27

The addition of CO also led to loss of ethylene uptake at 80 °C, with a loss of ethylene/Pd ratio by about ~1.2. We speculate that inclusion of CO in dry conditions results in competitive adsorption over the Pd sites responsible for ethylene uptake. Further, we found that the addition of H_2O and CO lead to almost complete loss of ethylene uptake. According to Table 1, under CO and H_2O co-feed, the catalyst displays ~7.5% of the ethylene uptake compared with the experiment with no H_2O and no CO. By combining the effects of H_2O and CO separately, these account for a loss of ~83% of ethylene storage. The remaining discrepancy, roughly 10% of total ethylene storage, is left unaccounted for.

Dodecane displays a different response to CO co-feed. We reported previously that while H_2O does affect dodecane uptake, it is only a slight effect, and the overall capacity remains high [16]. As shown in Figure 3, dodecane uptake displays no appreciable response to CO. This is reasonable as we expect that CO should have no effect on dodecane uptake since there is no interaction between dodecane and the Pd active sites. The dodecane uptake mechanism relies on its condensation within the zeolite pores, with only Van der Waals forces between dodecane and the pore walls.

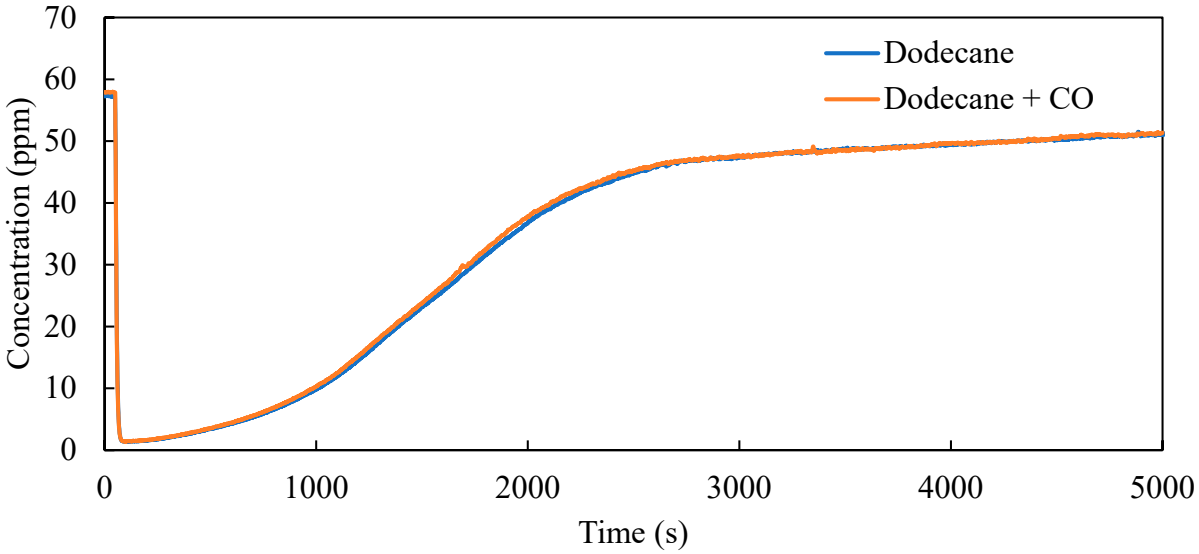

Figure 3. Dodecane uptake over 1% Pd/BEA with and without CO co-feed. (58 ppm $C_{12}H_{26}$, 0 or 500 ppm CO, 6% H_2O, 12% O_2, balance N_2).

2.3. Temperature Programmed Oxidation

TPO studies were conducted to simulate the warmup of the exhaust due to engine load. Figure 4 shows the outlet ethylene concentration during the temperature ramp under several feed conditions. When H_2O is included, but CO absent, ethylene oxidation light-off occurred at the highest temperature, with the temperature at 50% inlet ethylene conversion (T_{50}) near 320 °C. Additionally, a sustained low level of conversion can be observed. This corresponds to the formation of acetaldehyde, shown in Figure S1, demonstrating that catalytic partial oxidation occurs, potentially through Wacker chemistry involving ionic Pd and H_2O. Recent work on Pd-Cu/Y zeolites found that Wacker chemistry is feasible under similar conditions. In our work however, the rate of acetaldehyde formation is hindered by the lack of Cu^{2+}. Although molecular O_2 can oxidize Pd in these conditions, Pd oxidation by Cu^{2+} was highlighted as an important step in recent Wacker chemistry literature [35,36].

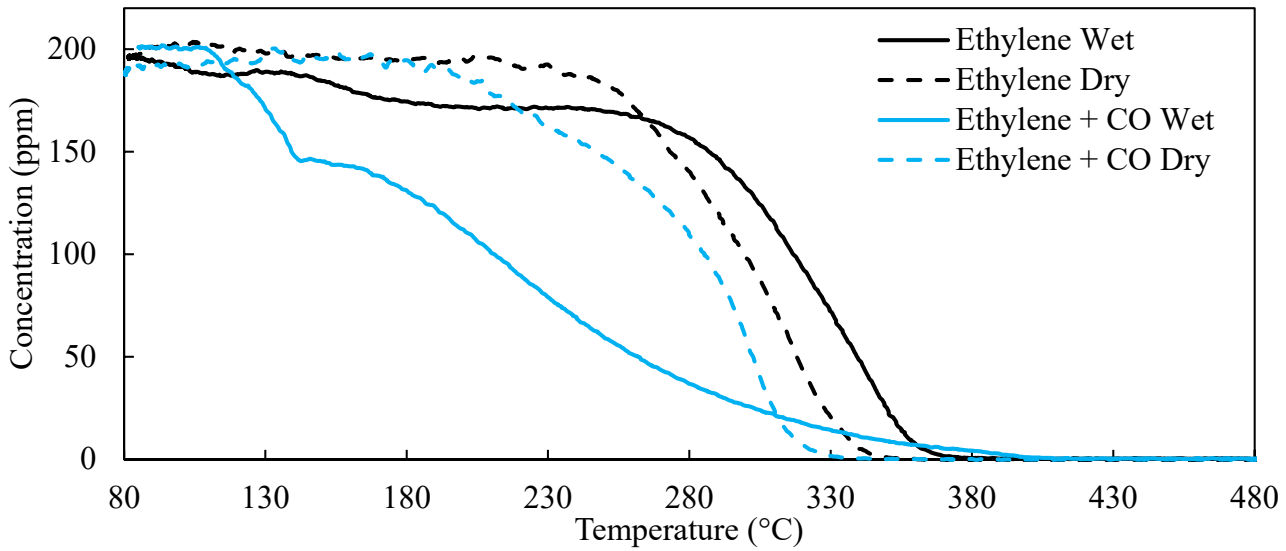

Figure 4. Ethylene conversion during a temperature ramp with and without CO under wet and dry conditions (200 ppm ethylene, 0 or 500 ppm CO, 0 or 6% H_2O, 12% O_2, balance N_2).

When including CO with the ethylene and H_2O, ethylene oxidation follows a non-standard light-off profile, with a non-monotonic change around 140 °C. This feature is likely due to additional ethylene uptake over Pd sites as CO desorbs. Zheng et al. performed a CO TPD over 0.92% Pd/BEA, taking IR spectra every 50 °C. They found that bands representing CO adsorbed to various Pd species began to rapidly diminish starting at 150 °C [25]. Their result is in agreement with our observation of ethylene adsorbing to the sites which were freed up by CO desorption around 150 °C. The overlaid CO concentration profiles are plotted in Figure S2, showing CO oxidation light-off occurs just before this reuptake feature. After this reuptake feature, ethylene conversion follows the standard light-off profile, with a T_{50} = 210 °C, but does not reach complete conversion until 400 °C, higher than under the ethylene and H_2O, absent CO, feed conditions.

Under dry conditions, we do not observe the reuptake feature, and the effect of CO on ethylene oxidation is not as significant as observed under wet conditions. With dry ethylene feed, the acetaldehyde formation no longer occurs, since Wacker chemistry reactant H_2O is absent. Instead, conversion remains near zero until 250 °C, when a typical oxidation curve forms, with T_{50} near 300 °C. When CO is added to the dry ethylene feed, oxidation activity improves slightly. This may be due to an exotherm effect from the CO conversion. It also may be due to reduced ethylene uptake, as high ethylene coverage may self-inhibit the oxidation reaction [37,38].

Similar experiments were conducted with dodecane as the model hydrocarbon. Results are shown in Figure 5. Intermediate smaller chain hydrocarbons are observed during the temperature ramp, which is due to dodecane undergoing a cracking reaction within the zeolite as the temperature rises. The hydrocarbons which we observed include ethylene, propylene, and isobutylene, but here we group them together and labeled them as 'Cracking Products'. We speculate that alkenes produced by this reaction bond to Pd^{2+} via π-electron interactions, resulting in a degree of retention via chemisorption. Previously, we reported that over a Pd/BEA hydrocarbon trap, the desorption temperature of the remaining trapped hydrocarbons is coupled with the exotherm produced during oxidation [16]. Therefore, the oxidation ability of the hydrocarbon trap contributes to the overall performance in low temperature hydrocarbon abatement.

In Figure 5a, cracking products can be observed starting at 190 °C. The appearance of these species, plotted on a C_{12} basis, mirrors the decrease in dodecane signal until oxidation occurs and the exotherm generated results in desorption of the remaining hydrocarbons, with some being oxidized in the process. Under CO co-feed conditions, Figure 5b, this exotherm occurs 50 °C lower, at 200 °C instead of 250 °C. The decreased oxidation light-off temperature is unlikely to be due to an exotherm generated solely by CO oxidation since the adiabatic temperature rise for 500 ppm CO is about 5 °C. This is the same behavior observed during ethylene uptake and TPO.

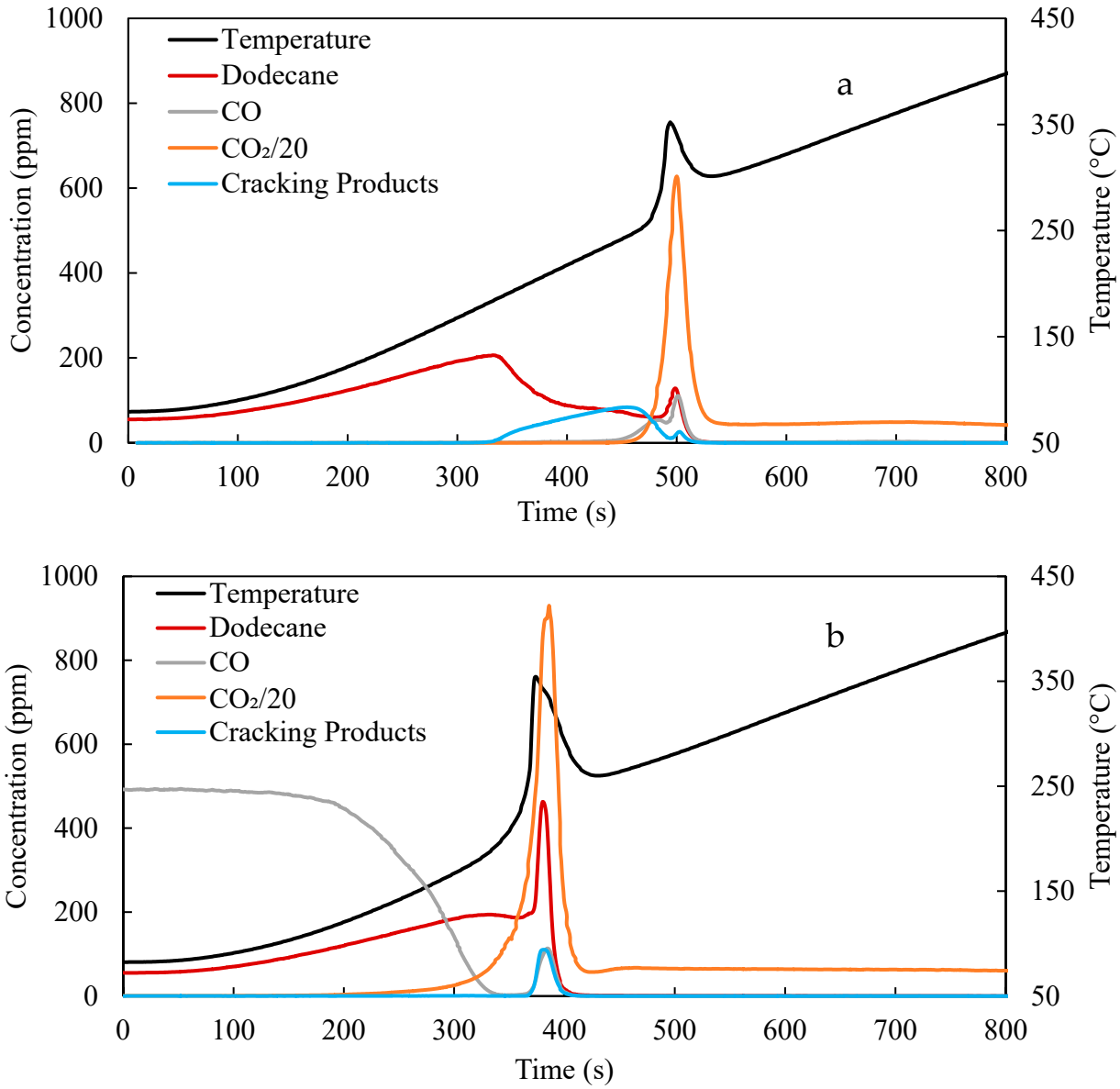

Figure 5. TPO Profiles of (**a**) Dodecane, (**b**) Dodecane + CO (58 ppm $C_{12}H_{26}$, 0 or 500 ppm CO, 6% H_2O, 12% O_2, balance N_2).

2.4. CO Pretreatment

In an effort to further isolate the effects of CO and H_2O, we subjected the catalyst to two pretreatments. The first was a 30-min 500 ppm CO pretreatment in 12% O_2 and balance N_2. The second was a 30-min 500 ppm CO pretreatment in 6% H_2O, 12% O_2, and balance N_2. After each individual pretreatment, we performed the ethylene adsorption and TPO experiment. Figure 6 shows the ethylene oxidation light-off curves after each pretreatment and compares these results to the oxidation light-off curves for ethylene in wet and dry conditions without any pretreatment.

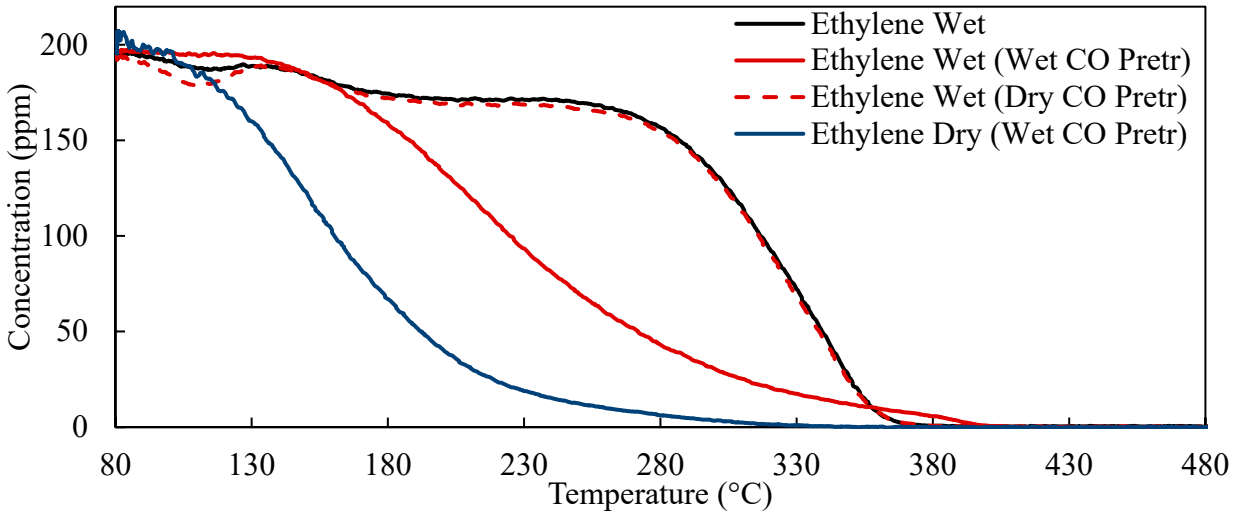

Figure 6. Ethylene conversion during temperature ramp after wet and dry CO pretreatment. (Pretreatment: 500 ppm CO, 0 or 6% H_2O, 12% O_2, balance N_2) (Adsorption and TPO: 200 ppm ethylene, 0 or 500 ppm CO, 0 or 6% H_2O, 12% O_2, balance N_2).

There are differences in these data at temperatures below 130 °C, which are due to desorption of H_2O and the resulting uptake of ethylene which leads to an apparent conversion. Above 130 °C, the changes are due to oxidation. The dashed red line, which represents the ethylene oxidation curve in the presence of H_2O, but after a dry CO pretreatment, overlaps almost completely above 130 °C with the solid black line representing the ethylene TPO in the presence of H_2O. A dry CO pretreatment has no effect on the oxidation behavior of the Pd catalyst.

Above 130 °C, the oxidation curve after a wet CO pretreatment, red solid line, mimics the exact behavior as the wet CO co-feed experiment, Figure 4 solid blue line, with the exception of the uptake feature peaking at 140 °C, which is absent here because CO is not in the feed during the uptake and TPO. By replicating the same oxidation light-off curve, even with no CO present during the hydrocarbon adsorption and TPO, we hypothesize that a wet CO co-feed alters the Pd/BEA hydrocarbon trap in some way which enhances hydrocarbon oxidation activity. These changes in oxidation activity however are reversible by O_2 treatment at 600 °C. Each experiment could be replicated regardless of the order in which they were conducted.

If we pretreat the catalyst with CO and H_2O and then remove both from the feed, the blue oxidation light-off curve is generated. Compared with the dry ethylene feed experiment (Figure 4), the T_{50} is 140 °C lower. These results suggest that the altered Pd phase responsible for the enhanced oxidation is inhibited by H_2O. Curiously, the removal of H_2O from the feed in experiments without the CO/H_2O pretreatment, Figure 4 dashed lines, did not lead to as severe an increase in oxidation activity. The overall oxidation activity based on reaction conditions can be summarized in ascending order of T_{50} as follows:

Ethylene (CO/H_2O pretreatment) > Ethylene/H_2O (CO/H_2O pretreatment) = Ethylene/CO/ H_2O > Ethylene/CO > Ethylene > Ethylene/H_2O.

Clearly, the coexistence of CO and H_2O at 80 °C changes the oxidation activity of the Pd catalyst, because ethylene single feed improves from nearly the worst in ethylene oxidation performance to the best after pretreatment in CO/H_2O. The changes made by this pretreatment are of importance to study, as under normal engine conditions, these components will be part of the gas mixture at these temperatures.

2.5. CO DRIFTS

To further investigate the changes on the catalyst by co-feeding CO and H_2O, we used DRIFTS with CO as the probe molecule. Four experiments were conducted consecutively in

the following sequence, Dry 1→Wet 2→Dry 3→Wet 4, with 'Dry' experiments containing no H_2O in the feed. The results, shown in Figure 7, indicate that many CO–Pd species exist on the Pd/BEA catalyst at 80 °C. The first dry spectrum, labeled 'Dry 1', displays features at 2214 and 2194 cm^{-1} which correspond to CO bound to 'super electrophilic' Pd^{2+} [39]. These features, seemingly unstable, appear and grow very quickly upon CO exposure then slowly decrease after 10 min CO exposure (Figure S3). Additional features, which have been assigned to CO–Pd^{2+}, appear at 2180, 2173, 2153, and 2140 cm^{-1}. The feature appearing at 2120 cm^{-1} is often attributed to CO–Pd^{+} [24,25,40–42]. Finally, two peaks at 2098 and 2080 cm^{-1}, which correspond to linearly bound CO–Pd^{0}, appear after approximately 30 min exposure. These are likely formed upon reduction by the probe molecule, CO, during exposure and thus not indicative of isolated Pd^{0} in the oxidized sample [25,41]. Under dry conditions no peaks appear in the range of 1800–2000 cm^{-1}.

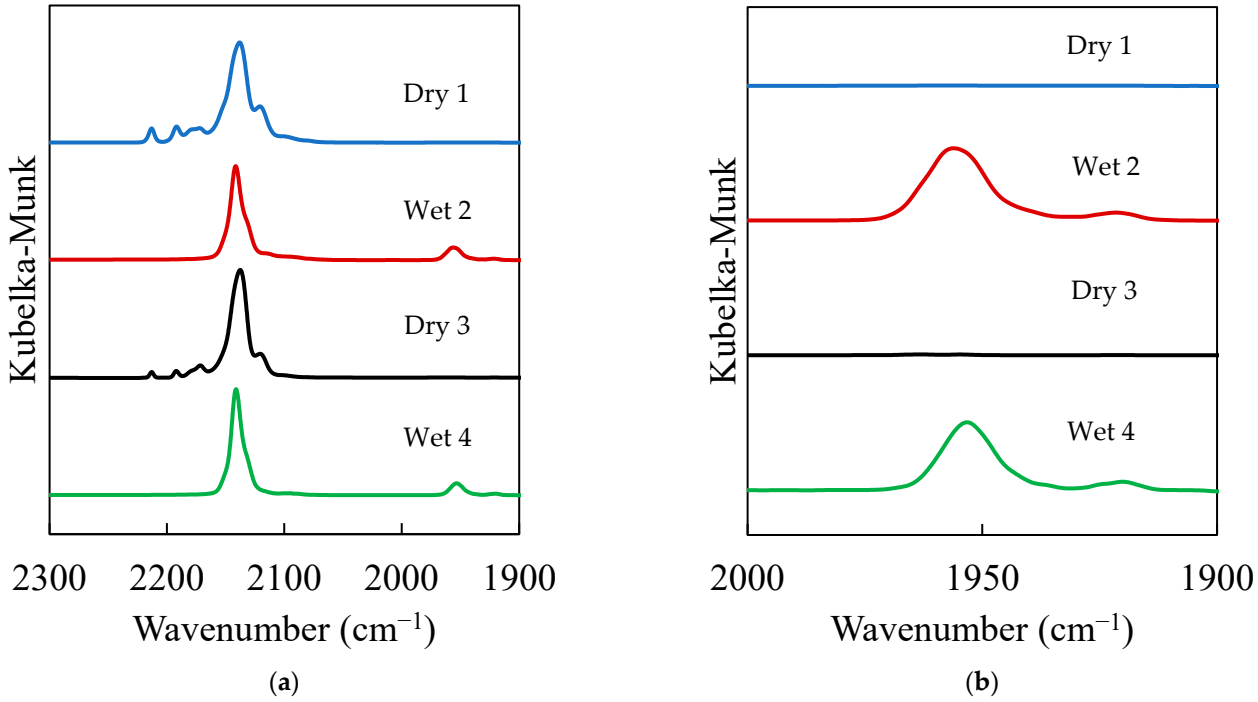

Figure 7. CO DRIFTS at 80 °C with four consecutive experiments switching between dry and wet conditions, with O_2 pretreatments at 500 °C in between each. (**a**) Showing the region depicting ionic and reduced Pd species. (**b**) Zoomed in to the region where CO-Pd_2 peaks arise. Exposure time = 30 min. (1000 ppm CO, 2% H_2O, 10% O_2, balance He).

Under wet conditions, fewer ionic Pd^{2+} peaks appear. In the 'Wet 2' spectrum, the only remaining peaks which correspond to Pd^{2+} are at 2153 and 2140 cm^{-1}. A peak emerges at 2125 cm^{-1} which may correspond to a blue shifted 2120 cm^{-1} peak. Peaks at 2098 and 2080 cm^{-1} remain, but again do not populate until much later times, after 30 min exposure to CO and H_2O. Most interestingly, peaks at 1920 and 1950 cm^{-1} emerge and grow over the course of the experiment (Figure S4). These correspond to bridging CO–Pd_2^0 which can only occur over Pd particles [28,41–44]. The following two spectra, "Dry 3" and "Wet 4", demonstrate the ability to replicate the same CO–Pd environment after multiple cycles.

The H_2 TPR experiment, Figure 1, indicated that a particulate phase exists on the surface of the sample. After oxidative pretreatment at 500 °C, these particles would exist as PdO, and thus would not be detected by CO adsorption DRIFTS. By reducing the sample at 500 °C in H_2 after O_2 treatment, and subsequent adsorption by CO at 80 °C, we detected bridging CO–Pd_2 and three-fold CO–Pd_3, Figure S5. Due to the heterogeneous nature of our as-synthesized catalyst, that is the existence of particulate Pd and ionic Pd, it is unclear whether the newly formed bridging CO–Pd_2 sites stem from partially reduced PdO or the formation of an agglomerated Pd phase within the zeolite pores. Further studies with a

model Pd/BEA catalyst are required to understand the mechanism behind this change in the Pd speciation.

3. Materials and Methods

3.1. Catalyst Synthesis

Zeolite beta with Si/Al = 19 was purchased in the ammonium cation form (CP814C, Zeolyst International, Conshohocken, PA, USA). The catalyst powder was calcined at 500 °C for 4 h in air to obtain the H^+ form. Pd/BEA was synthesized from the H^+ form catalyst by incipient wetness impregnation. An appropriate amount of $Pd(NO_3)_2$ (Sigma Aldrich, St. Louis, MO, USA) was dissolved in water and mixed with the zeolite powder in a dropwise fashion to achieve 1 wt% Pd by mass. The resulting catalyst was calcined at 600 °C for 4 h in air. Cordierite monoliths (300 cells/in^2) were washcoated with Pd/BEA. The washcoat slurry was prepared by first mixing the catalyst powder, sieved to 60–80 mesh, with a colloidal alumina binding agent (Nyacol Al20, Nyacol Nano Technologies Inc., Ashland, MA, USA) and water. The resulting slurry was then wash coated onto a ~4 cm long by 0.75 cm diameter monolith substrate several times in an iterative process where the monolith was dipped and dried several times until the desired loading of 1 g/in^3 was achieved. The monoliths were then dried at 120 °C for 2 h and calcined at 600 °C for 4 h in air at a ramp rate of 1 °C/min.

3.2. Catalyst Characterization

Hydrogen temperature programmed reduction (TPR) was performed on an AutoChem II 2920 chemisorption analyzer (Micromeritics Instruments Corporation, Norcross, GA, USA). As-synthesized Pd/BEA powder was placed in a tube with a thermocouple inserted directly on top of the powder. The catalyst was subjected to a 45-min pretreatment in 10% O_2 in a balance of N_2 at 500 °C before undergoing the TPR experiment in 5% H_2 in a balance of N_2 starting at 50 °C and ramping to 600 °C at a rate of 10 °C/min. The resulting thermal conductivity detector (TCD) signal correlates to the H_2 consumption as a function of temperature.

3.3. Reactor Tests

Catalysts were evaluated using a bench top reactor system. The monolith was placed in a quartz tube (Quartz Scientific Inc., Fairport Harbor, OH, USA) with thermocouples inserted into the upstream and downstream ends. The quartz tube was placed into a programmable furnace (Thermo Fisher Scientific, Waltham, MA, USA) for heating and temperature control. The reactor is equipped with a bypass line and two automated three-way valves upstream and downstream of the catalyst. The bypass allows for verification of the inlet gas concentrations. The automated valves provide instant introduction of the simulated exhaust mixture to the reactor. Gas phase concentrations were measured with Fourier transform infrared spectroscopy (FTIR) using an MKS 2030 series FTIR (MKS Instruments Inc., Andover, MA, USA). Due to overlapping spectral features of some hydrocarbon species, we combined ethylene, propylene, and isobutylene into one category which we labeled 'Cracking Products' in the plots below. The plotted concentrations of these cracking products are on a C_{12} basis to enable comparison to dodecane concentrations.

Gas phase reactants were all supplied using gas cylinders (Praxair Inc. Danbury, CT, USA), except for water and dodecane. Water was introduced using a controlled evaporator mixer (Bronkhorst, Ruulo, The Netherlands), while dodecane was added using a bubbler with nitrogen as the carrier gas. The gas hourly space velocity was 30,000 hr^{-1} for all experiments in the bench top reactor. Adsorption-desorption experiments followed the protocol outlined in Figure 8.

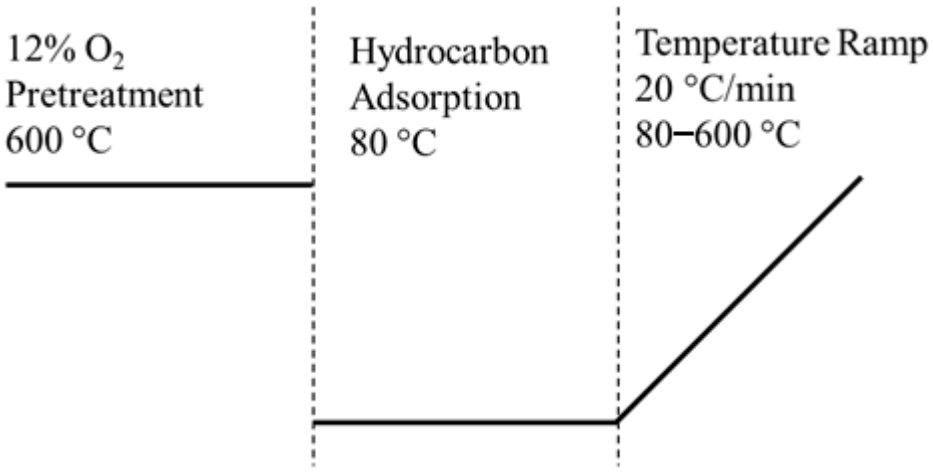

Figure 8. Adsorption-desorption protocol.

The monolith was pretreated in 12% O_2 in balance N_2 at 600 °C for 1 h to remove any carbon from previous experiments and reoxidize the Pd in the zeolite. During the oxidizing pretreatment, the simulated exhaust gas was established in the bypass line. Table 2 outlines the gas phase species concentrations used in this work.

Table 2. Feed gas concentration for each species.

Species	Concentration
N_2	Balance
O_2	12%
H_2O	6%
CO	500 ppm
C_2H_4	200 ppm
$C_{12}H_{26}$	58 ppm

After the oxygen pretreatment, the temperature was stabilized at 80 °C in the furnace. When the temperature was stable, and the simulated exhaust was stable in the bypass, the valves were switched and the exhaust mixture was flowed to the catalyst. The adsorption phase was 30 min for ethylene and 2 h for dodecane, both times were well after the hydrocarbon had fully saturated the catalyst based on the effluent concentration equaling the inlet. Immediately after this period, the temperature ramp began, where the catalyst was heated from 80 to 600 °C at a rate of 20 °C/min.

3.4. DRIFTS Studies

DRIFTS was used to investigate the Pd speciation upon introduction of CO with and without the presence of H_2O. The powder Pd/BEA was placed in a Harrick Scientific Praying Mantis reaction chamber (Harrick Scientific Products Inc., Pleasantville, NY, USA) with ZnSe windows. The instrument used was a Nicolet iS50 FT-IR (Thermo Fisher Scientific, Waltham, MA, USA). Each experiment began with a 500 °C pretreatment in 10% O_2/He for 45 min. The cell was then cooled to 80 °C in the same mixture. For the hydrogen reduced sample, the O_2 pretreatment was followed by a 45-min treatment in a 2% H_2/He mixture at 500 °C. This sample was then cooled to 80 °C in He.

For the dry experiments a background spectrum was taken in He/O_2 when stable. Under wet conditions, 2% H_2O was added to the mixture via a bubbler, with the concentration confirmed with the MKS 2030 FTIR, and a background spectrum was taken when stable. For the H_2 reduced sample, the background spectrum was taken in He. Finally, 1000 ppm CO was introduced to the mixture and sample spectra were taken initially every minute

for 10 min followed by every 5 min until an hour elapsed. For each reported spectrum, 32 spectra were averaged.

4. Conclusions

In this work, we conducted hydrocarbon trap experiments over Pd/BEA and varied the feed composition to test the effects of H_2O and CO. Dodecane uptake was not inhibited by H_2O or CO co-feed, but ethylene uptake was significantly affected by both. In fact, when H_2O and CO both existed in the feed, ethylene uptake was decreased by over 90% compared to the uptake with both absent. Ethylene uptake loss when CO is present is likely due to competitive adsorption to ionic Pd sites, and ethylene uptake loss when H_2O is present is likely due to competitive adsorption to Brønsted acid sites. When CO and H_2O are co-fed, however, the larger decrease in ethylene uptake occurred which may result from the formation of reduced Pd which is inactive in ethylene uptake.

Temperature programmed oxidation experiments revealed a similar effect of CO and H_2O on both ethylene and dodecane desorption and oxidation. When CO and H_2O were both present in the mixture, hydrocarbon oxidation occurred at much lower temperatures than with any other combination of feed. When subjected to pretreatment in CO, differences in TPO behavior only occurred when the pretreatment contained both CO and H_2O.

CO-DRIFTS results show that under conditions that include H_2O conditions, peaks arise which indicate bridging CO–Pd_2^0. These represent a reduced Pd phase which we speculate led to the enhanced hydrocarbon oxidation activity.

Supplementary Materials: The following are available online at https://www.mdpi.com/2073-4344/11/3/348/s1, Figure S1: Outlet gas concentrations during TPO for a wet ethylene feed mixture, Figure S2: Outlet gas concentrations during TPO for a wet ethylene and CO feed mixture, Figure S3: CO DRIFTS spectra over 1% Pd/BEA of 'Dry 1′ time resolved, Figure S4: CO DRIFTS spectra over 1% Pd/BEA of 'Wet 2′ time resolved, Figure S5: CO DRIFTS spectra over 1% Pd/BEA after 500 °C pretreatment in 2% H_2, Figure S6: CO TPR under wet conditions, Figure S7: Ethylene TPR under wet conditions, Figure S8: Ethylene co-fed with H_2 under wet conditions.

Author Contributions: Conceptualization, R.Z. and W.S.E.; validation, R.Z; investigation, R.Z.; writing—original draft preparation, R.Z.; writing—review and editing, W.S.E.; visualization, R.Z and W.S.E.; supervision, W.S.E.; project administration, W.S.E.; funding acquisition, W.S.E. All authors have read and agreed to the published version of the manuscript.

Funding: This research was funded by the Department of Energy, Vehicle Technologies Office, grant number DE-EE0008233.

Data Availability Statement: All data supporting our conclusions is shown in the paper, additional full datasets are available upon reasonable request to the corresponding author.

Conflicts of Interest: The authors declare no conflict of interest. The funders had no role in the design of the study; in the collection, analyses, or interpretation of data; in the writing of the manuscript, or in the decision to publish the results.

References

1. Wimmer, A.; Eichlseder, H.; Klell, M.; Figer, G. Potential of HCCI concepts for DI diesel engines. *Int. J. Veh. Des.* **2006**, *41*, 32–48. [CrossRef]
2. Heck, R.M.; Farrauto, R.J. Automobile exhaust catalysts. *Appl. Catal. A Gen.* **2001**, *221*, 443–457. [CrossRef]
3. Hochmuth, J.K.; Burk, P.L.; Tolentino, C.; Mignano, M.J. Hydrocarbon Traps for Controlling Cold Start Emissions. In Proceedings of the International Congress and Exposition, Detroit, MI, USA, 1–5 March 1993. [CrossRef]
4. Elangovan, S.P.; Ogura, M.; Davis, M.E.; Okubo, T. SSZ-33: A Promising Material for Use as a Hydrocarbon Trap. *J. Phys. Chem. B* **2004**, *108*, 13059–13061. [CrossRef]
5. Burke, N.; Trimm, D.; Howe, R. The effect of silica:alumina ratio and hydrothermal ageing on the adsorption characteristics of BEA zeolites for cold start emission control. *Appl. Catal. B Environ.* **2003**, *46*, 97–104. [CrossRef]
6. Yeon, T.H.; Han, H.S.; Park, E.D.; Yie, J.E. Adsorption and desorption characteristics of hydrocarbons in multi-layered hydrocarbon traps. *Microporous Mesoporous Mater.* **2009**, *119*, 349–355. [CrossRef]
7. Sarshar, Z.; Zahedi-Niaki, M.; Huang, Q.; Eić, M.; Kaliaguine, S. MTW zeolites for reducing cold-start emissions of automotive exhaust. *Appl. Catal. B Environ.* **2009**, *87*, 37–45. [CrossRef]

8. Westermann, A.; Azambre, B.; Finqueneisel, G.; Da Costa, P.; Can, F. Evolution of unburnt hydrocarbons under "cold-start" conditions from adsorption/desorption to conversion: On the screening of zeolitic materials. *Appl. Catal. B Environ.* **2014**, *158–159*, 48–59. [CrossRef]
9. Heimrich, M.J.; Smith, L.R.; Kitowski, J. Cold-Start Hydrocarbon Collection for Advanced Exhaust Emission Control. In Proceedings of the International Congress and Exposition, Detroit, MI, USA, 24–28 February 1992. [CrossRef]
10. Liu, X.; Lampert, J.K.; Arendarskiia, D.A.; Farrauto, R.J. FT-IR spectroscopic studies of hydrocarbon trapping in Ag+-ZSM-5 for gasoline engines under cold-start conditions. *Appl. Catal. B Environ.* **2001**, *35*, 125–136. [CrossRef]
11. Elangovan, S.; Ogura, M.; Ernst, S.; Hartmann, M.; Tontisirin, S.; Davis, M.E.; Okubo, T. A comparative study of zeolites SSZ-33 and MCM-68 for hydrocarbon trap applications. *Microporous Mesoporous Mater.* **2006**, *96*, 210–215. [CrossRef]
12. Gies, H.; van Koningsveld, H. Faulted Zeolite Framework Structures. In Proceedings of the 12th International Zeolite Con-ference, Baltimore, MD, USA, 5–10 July 1998; p. 2999.
13. Rollmann, L.D.; Valyocsik, E.W.; Shannon, R.D. Zeolite Molecular Sieves. In *Inorganic Syntheses*; Rovert, E., Ed.; Krieger Publishing Company Inc.: Malabar, FL, USA, 2006; Volume 22, ISBN 9780470132531.
14. Temerev, V.L.; Vedyagin, A.A.; Afonasenko, T.N.; Iost, K.N.; Kotolevich, Y.S.; Baltakhinov, V.P.; Tsyrulnikov, P.G. Effect of Ag loading on the adsorption/desorption properties of ZSM-5 towards toluene. *React. Kinet. Mech. Catal.* **2016**, *119*, 629–640. [CrossRef]
15. Kang, S.B.; Kalamaras, C.; Balakotaiah, V.; Epling, W. Hydrocarbon Trapping over Ag-Beta Zeolite for Cold-Start Emission Control. *Catal. Lett.* **2017**, *147*, 1355–1362. [CrossRef]
16. Zelinsky, R.; Epling, W. Effects of Multicomponent Hydrocarbon Feed on Hydrocarbon Adsorption–Desorption and Oxidation Light-Off Behavior on a Pd/BEA Hydrocarbon Trap. *Catal. Lett.* **2019**, *149*, 3194–3202. [CrossRef]
17. Xu, L.; Lupescu, J.; Cavataio, G.; Guo, K.; Jen, H. The Impacts of Pd in BEA Zeolite on Decreasing Cold-Start NMOG Emission of an E85 Fuel Vehicle. *SAE Int. J. Fuels Lubr.* **2018**, *11*, 239–246. [CrossRef]
18. Park, J.-H.; Park, S.J.; Ahn, H.A.; Nam, I.-S.; Yeo, G.K.; Kil, J.K.; Youn, Y.K. Promising zeolite-type hydrocarbon trap catalyst by a knowledge-based combinatorial approach. *Microporous Mesoporous Mater.* **2009**, *117*, 178–184. [CrossRef]
19. Westermann, A.; Azambre, B.; Chebbi, M.; Koch, A. Modification of Y Faujasite zeolites for the trapping and elimination of a propene-toluene-decane mixture in the context of cold-start. *Microporous Mesoporous Mater.* **2016**, *230*, 76–88. [CrossRef]
20. Xu, L.; Lupescu, J.; Ura, J.; Harwell, A.; Paxton, W.A.; Nunan, J.; Alltizer, C. Benefits of Pd Doped Zeolites for Cold Start HC/NOx Emission Reductions for Gasoline and E85 Fueled Vehicles. *SAE Int. J. Fuels Lubr.* **2018**, *11*, 301–317. [CrossRef]
21. Lupescu, J.; Xu, L.; Jen, H.-W.; Harwell, A.; Nunan, J.; Alltizer, C.; Denison, G. A New Catalyzed HC Trap Technology that Enhances the Conversion of Gasoline Fuel Cold-Start Emissions. *SAE Int. J. Fuels Lubr.* **2018**, *11*, 411–425. [CrossRef]
22. Kofke, T.J.G. A temperature-programmed desorption study of olefin oligomerization in H-ZSM-5. *J. Catal.* **1989**, *115*, 233–243. [CrossRef]
23. Malamis, S.A.; Harold, M.P.; Epling, W.S. Coupled NO and C_3H_6 Trapping, Release and Conversion on Pd/BEA: Evaluation of the Lean Hydrocarbon NOx Trap. *Ind. Eng. Chem. Res.* **2019**, *58*, 22912–22923. [CrossRef]
24. Zhang, B.; Shen, M.; Wang, J.; Wang, J.; Wang, J. Investigation of Various Pd Species in Pd/BEA for Cold Start Application. *Catalysts* **2019**, *9*, 247. [CrossRef]
25. Zheng, Y.; Kovarik, L.; Engelhard, M.H.; Wang, Y.; Wang, Y.; Gao, F.; Szanyi, J. Low-Temperature Pd/Zeolite Passive NOx Adsorbers: Structure, Performance, and Adsorption Chemistry. *J. Phys. Chem. C* **2017**, *121*, 15793–15803. [CrossRef]
26. Gu, Y.; Zelinsky, R.P.; Chen, Y.-R.; Epling, W.S. Investigation of an irreversible NOx storage degradation Mode on a Pd/BEA passive NOx adsorber. *Appl. Catal. B Environ.* **2019**, *258*, 118032. [CrossRef]
27. Vu, A.; Luo, J.; Li, J.; Epling, W.S. Effects of CO on Pd/BEA Passive NOx Adsorbers. *Catal. Lett.* **2017**, *147*, 745–750. [CrossRef]
28. Khivantsev, K.; Jaegers, N.R.; Kovarik, L.; Hanson, J.C.; Tao, F.; Tang, Y.; Zhang, X.; Koleva, I.Z.; Aleksandrov, H.A.; Vayssilov, G.N.; et al. Achieving Atomic Dispersion of Highly Loaded Transition Metals in Small-Pore Zeolite SSZ-13: High-Capacity and High-Efficiency Low-Temperature CO and Passive NOx Adsorbers. *Angew. Chem.* **2018**, *130*, 16914–16919. [CrossRef]
29. Khivantsev, K.; Jaegers, N.R.; Kovarik, L.; Prodinger, S.; Derewinski, M.A.; Wang, Y.; Gao, F.; Szanyi, J. Palladium/Beta zeolite passive NOx adsorbers (PNA): Clarification of PNA chemistry and the effects of CO and zeolite crystallite size on PNA performance. *Appl. Catal. A Gen.* **2019**, *569*, 141–148. [CrossRef]
30. Ryou, Y.; Lee, J.; Kim, Y.; Hwang, S.; Lee, H.; Kim, C.H.; Kim, D.H. Effect of reduction treatments (H_2 vs. CO) on the NO adsorption ability and the physicochemical properties of Pd/SSZ-13 passive NOx adsorber for cold start application. *Appl. Catal. A Gen.* **2019**, *569*, 28–34. [CrossRef]
31. Theis, J.R.; Ura, J.A. Assessment of zeolite-based Low temperature NOx adsorbers: Effect of reductants during multiple sequential cold starts. *Catal. Today* **2021**, *360*, 340–349. [CrossRef]
32. Nag, N.K. A Study on the Formation of Palladium Hydride in a Carbon-Supported Palladium Catalyst. *J. Phys. Chem. B* **2001**, *105*, 5945–5949. [CrossRef]
33. Han, D.; Ickes, A.M.; Bohac, S.V.; Huang, Z.; Assanis, D.N. HC and CO emissions of premixed low-temperature combustion fueled by blends of diesel and gasoline. *Fuel* **2012**, *99*, 13–19. [CrossRef]
34. Iliyas, A.; Zahedi-Niaki, H.; Eić, M. One-dimensional molecular sieves for hydrocarbon cold-start emission control: Influence of water and CO_2. *Appl. Catal. A Gen.* **2010**, *382*, 213–219. [CrossRef]

35. Imbao, J.; Van Bokhoven, J.A.; Nachtegaal, M. Optimization of a heterogeneous Pd–Cu/zeolite Y Wacker catalyst for ethylene oxidation. *Chem. Commun.* **2020**, *56*, 1377–1380. [CrossRef]
36. Imbao, J.; Van Bokhoven, J.A.; Clark, A.; Nachtegaal, M. Elucidating the mechanism of heterogeneous Wacker oxidation over Pd-Cu/zeolite Y by transient XAS. *Nat. Commun.* **2020**, *11*, 1–9. [CrossRef]
37. Daneshvar, K.; Dadi, R.K.; Luss, D.; Balakotaiah, V.; Kang, S.B.; Kalamaras, C.M.; Epling, W.S. Experimental and modeling study of CO and hydrocarbons light-off on various Pt-Pd/γ-Al2O3 diesel oxidation catalysts. *Chem. Eng. J.* **2017**, *323*, 347–360. [CrossRef]
38. Bugosh, G.S.; Harold, M.P. Impact of Zeolite Beta on Hydrocarbon Trapping and Light-Off Behavior on Pt/Pd/BEA/Al_2O_3 Monolith Catalysts. *Emiss. Control Sci. Technol.* **2017**, *3*, 123–134. [CrossRef]
39. Khivantsev, K.; Jaegers, N.R.; Koleva, I.Z.; Aleksandrov, H.A.; Kovarik, L.; Engelhard, M.H.; Gao, F.; Wang, Y.; Vayssilov, G.N.; Szanyi, J. Stabilization of Super Electrophilic Pd+2 Cations in Small-Pore SSZ-13 Zeolite. *J. Phys. Chem. C* **2020**, *124*, 309–321. [CrossRef]
40. Zhanga, Y.; Fulajtárová, K.; Kubůa, M.; Mazura, M.; Hronecb, M.; Čejka, J. Electronic/steric effects in hydrogenation of nitroarenes over the heterogeneous Pd@BEA and Pd@MWW catalysts. *Catal. Today* **2020**, *345*, 39–47. [CrossRef]
41. Kyriakidou, E.A.; Lee, J.; Choi, J.-S.; Lance, M.; Toops, T.J. A comparative study of silver- and palladium-exchanged zeolites in propylene and nitrogen oxide adsorption and desorption for cold-start applications. *Catal. Today* **2021**, *360*, 220–233. [CrossRef]
42. Xu, J.; Ouyang, L.; Mao, W.; Yang, X.-J.; Xu, X.-C.; Su, J.-J.; Zhuang, T.-Z.; Li, H.; Han, Y.-F. Operando and Kinetic Study of Low-Temperature, Lean-Burn Methane Combustion over a Pd/γ-Al_2O_3 Catalyst. *ACS Catal.* **2012**, *2*, 261–269. [CrossRef]
43. Aylor, A.W.; Lobree, L.J.; Reimer, J.A.; Bell, A.T. Investigations of the Dispersion of Pd in H-ZSM-5. *J. Catal.* **1997**, *172*, 453–462. [CrossRef]
44. Bensalem, A.; Muller, J.-C.; Tessier, D.; Bozon-Verduraz, F. Spectroscopic study of CO adsorption on palladium–ceria catalysts. *J. Chem. Soc. Faraday Trans.* **1996**, *92*, 3233–3237. [CrossRef]